Steering On-Surface Self-Assembly of High-Quality Hydrocarbon Networks with Terminal Alkynes

Nenad Kepčija,[†] Yi-Qi Zhang,[†] Martin Kleinschrodt,[†] Jonas Björk,[‡] Svetlana Klyatskaya,[§] Florian Klappenberger,*[,†] Mario Ruben,[§,‖] and Johannes V. Barth[†]

[†]Physik Department E20, Technische Universität München, James-Franck-Straße, 85748 Garching, Germany
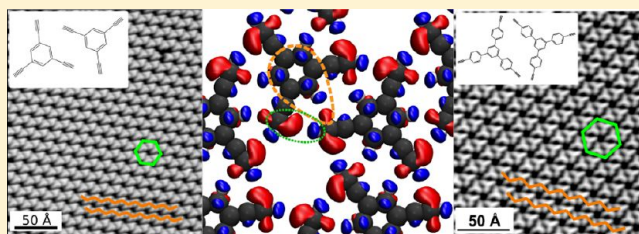[‡]Department of Physics, Chemistry and Biology (IFM), Linköping University, 58183 Linköping, Sweden
[§]Institute of Nanotechnology, Karlsruhe Institute of Technology, 76344 Eggenstein-Leopoldshafen, Germany
[‖]IPCMS-CNRS, Université de Strasbourg, 23 Rue de Loess, 67034 Strasbourg, France

Ⓢ *Supporting Information*

ABSTRACT: The two-dimensional (2D) self-assembly of 1,3,5-triethynyl-benzene (TEB) and *de novo* synthesized 1,3,5-tris-(4-ethynylphenyl)benzene (Ext-TEB) on Ag(111) was investigated by means of scanning tunneling microscopy (STM) under ultrahigh vacuum (UHV) conditions. Both 3-fold symmetric molecules form long-range ordered nano-porous networks featuring organizational chirality, mediated by novel, planar 6-fold cyclic binding motifs. The key interaction for the expression of the motifs is identified as C−H⋯π bonding. For Ext-TEB, an additional open-porous phase exists with the 3-fold motif. The nature of the underlying noncovalent bonding schemes is thoroughly analyzed by density functional theory (DFT) calculations including van der Waals corrections. The comparison of calculations focusing on isolated 2D molecular sheets and those including the substrate reveals the delicate balance between the attractive molecule−molecule interaction, mediated by both the terminal alkyne and the phenyl groups, and the molecule−substrate interaction responsible for the commensurability and the regularity of the networks. Comparison with bulk structures of similar molecules suggests that these strictly planar cyclic binding motifs appear only in 2D environments.

■ INTRODUCTION

Supramolecular chemistry has evolved into one of the most important approaches for the engineering of novel functional materials.[1−3] Among the possible noncovalent interactions hydrogen bonding is most suited because it provides selectivity and directionality combined with a reversible formation process.[4,5] For the rational design of crystal properties by supramolecular synthons, i.e., structural units that assemble by conceivable intermolecular interactions, a profound understanding of the driving forces behind the attraction between the numerous functional groups is mandatory.[6,7] Aside from the classical, strong hydrogen bridges, their C−H⋯π analogs, where an acidic CH moiety acts as proton donor and a weakly electron rich π-system plays the role of the acceptor, have been identified as versatile ingredients.[8,9]

In this context, terminal alkynes are especially interesting because they unite comparatively strong proton donor capabilities, which result from the high acidity of the alkynyl atom, with great versatility originating from the fact that their π system can simultaneously act as proton acceptor.[8,10] Initially, they have been recognized as secondary structural force in crystals of molecules featuring at the same time classical hydrogen bonding functionalities.[10−13] Later it was demonstrated that in the absence of such functionalities, the terminal alkyne interactions are the dominant ones.[14−16] It is worth

mentioning that the competing interaction with the π-system of an aromatic ring is not established in any of these crystal structures.[14−16] Often infinite zigzag patterns of nearly T-shaped arrangements of the ethyne groups are established,[10,12,14,15,17] but also three- and six-membered synthons have been reported.[15,17,18] A somewhat controversially discussed topic is the manifestation of the cooperative effect, i.e., an increase of the binding energy per bond with increasing number of connected bonds,[10,19] in synthons built-up by terminal alkynes. On the one hand, cooperative stabilization is suggested by experimental results[10,12,15,20,21] as well as early quantum chemical calculations;[12] on the other hand, such effects are not found with the same methods in cases appearing quite similar.[13] A more recent theoretical investigation focusing on ethyne concluded that no cooperative effect appear in between C_2H_2 molecules and only small additional stabilization (10%) results in the presence of water.[22] It could be tentatively concluded from this discussion that the backbone to which terminal alkynes are attached might have a pronounced influence on the manifestation of cooperative gain.

With the aim of a purposeful creation of functional nanostructures on surfaces, considerable effort has been devoted to understand how synthons known from three-dimensional (3D) supramolecular chemistry adapt to the novel, two-dimensional (2D) environment.[23−25] Examples of binding motifs being successfully transferred into two dimensions include the classical O−H···N, N−H···O, and N−H···N hydrogen bridges.[26−29] Self-complementary multiple H bond synthons were used to create porous networks[30,31] or bicomponent lines[32] as well as to steer conformation-selective self-assembly.[33] Cyclic binding motifs were stabilized by benzonitrile interactions leading to controlled supramolecular aggregates[34] and regular porous networks of varying symmetry.[35,36] By contrast, terminal alkynes have so far been disregarded in the field of on-surface supramolecular chemistry. Accordingly, their properties when adsorbed on surfaces as well as their potential for steering the production of 2D structures are unknown. Only one, very recent study addresses the formation of regular hexameric aggregates of ethynylbenzene on Au(111).[37]

Here we contribute to filling this knowledge gap by presenting a systematic investigation of the self-assembly capabilities of multitopic terminal alkyne functionalized molecules in a 2D environment, namely, on the Ag(111) surface in ultrahigh vacuum (UHV) conditions. The triple bond of phenylacetylene often becomes transformed to a formally double bond due to adsorption on more reactive substrates such as Pt or Cu,[38−40] but it stays intact on Au(111).[37] Therefore it is an open question of whether the terminal alkynes preserve their supramolecular organization capabilities on the silver surface. Our low-temperature scanning tunneling microscopy (STM) reveals long-range ordered crystal-quality networks surface which are stabilized via novel, cyclic binding motifs and feature small nanopores. Using density functional theory (DFT) calculations we address the influence of the surface on the bonding capabilities of the ethyne moieties including the effect of cooperativity and discuss the delicate interplay between molecule−surface and intermolecular interactions leading to the extended supramolecular layer. Moreover, the present findings are potentially important regarding the homocoupling reaction occurring with the same building blocks at higher temperatures, which we reported recently.[41]

■ METHODS

Synthesis. The 1,3,5-triethynyl arenes were obtained by Pd/Cu-catalyzed Sonogashira cross-coupling reaction of aryl bromides and terminal alkyne-trimethylsilylacetylene in the presence of secondary amine as solvent and base. The resulting silyl-intermediates were hydrolyzed to yield 86% and 75% of 1,3,5-triethynylbenzene (TEB, **1**) and 1,3,5-tris-(4-ethynylphenyl)benzene (Ext-TEB, **2**), respectively.

STM Measurements. All measurements were performed in an UHV chamber (base pressure $< 2 \times 10^{-10}$ mbar). The clean Ag(111) single crystal surface was prepared by repeated cycles of Ar$^+$ sputtering and annealing to 740 K. Both types of molecules were sublimated by an organic molecular beam epitaxy (OMBE) from a quartz glass crucible inside a Knudsen cell stabilized at a temperature T_{OMBE}. The sublimation temperature of the TEB molecules was below $T_{OMBE} = 370$ K in order to avoid polymerization in the crucible. Ext-TEB molecules were deposited at $T_{OMBE} = 420-450$ K onto the substrate at T_{sub} as indicated. If no sample is present, the OMBE evaporates directly into a residual gas analyzer. It can

detect the partial pressure at the atomic mass of the molecules, which is used as a measure for the molecular flux. In UHV, the room temperature vapor pressure of TEB is finite. As a result, the molecular flux obtained at a specific T_{OMBE} reduces with time after filling of the crucible. After evaporation of the organic film, the samples were transferred into a homemade Besocke-type scanning tunneling microscope (STM) where they were cooled down to 5.5 K where data were recorded. The error bars of the measured values of the three models presented for the supramolecular structure were determined by standard deviation.
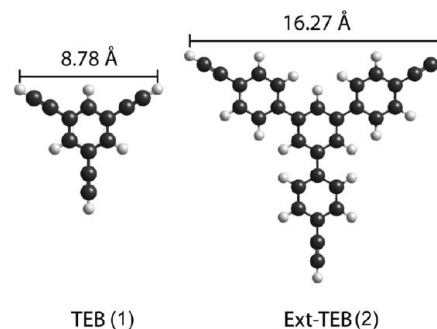
DFT Calculations. DFT calculations were performed within the VASP code,[42] with ion-core interaction described by the projector augmented wave method.[43,44] A variant of van der Waals density function[45] was used, with the exchange potential replaced by an optimized form of the Becke 86 functional.[46] The plane waves have been expanded to a cutoff of 500 eV. A $p(7 \times 7)$ unit cell together with a 2×2 k-point sampling was used in the calculations of single TEB molecules on Ag(111). For the TEB network, the unit cell determined experimentally was used, as specified in the text, together with a 3×3 k-point sampling. This ensures a convergence of binding energies within 10 meV, enabling the comparison of binding energies from calculations with different unit cells. The Ag(111) surface was modeled by a four-layered slab. All structures were geometrically optimized until the forces on atoms in the molecules and the two outermost surface layers were smaller than 0.01 eV/Å, while the two bottom slab layers were kept fixed.

HYPERCHEM Calculations. By means of the HYPERCHEM Software (HYPERCHEM, Hypercube Inc., Gainesville, FL) we calculated the models of TEB and Ext-TEB. Both geometries were optimized with semiempirical methods using the AM1 model.

■ RESULTS AND DISCUSSION

In order to study creation of networks based on interaction between terminal ethyne groups, we employed TEB (**1**) and Ext-TEB (**2**) (Scheme 1). TEB consists of a benzene ring with

Scheme 1. TEB and Ext-TEB

TEB (1)   Ext-TEB (2)

three acetylene groups attached to the carbon atoms in positions 1, 3, and 5. The molecule exhibits D_{3h} symmetry, and the distance between hydrogen atoms of the terminal alkyne groups amounts to 8.78 Å.

After 1 min exposure of the substrate at $T_{sample} = 180$ K, long-range ordered regular nanoporous networks were observed (Figure 1). In the STM images, the molecules appear as bright triangular protrusions. The triangles are arranged such that they form zigzag lines (orange), neighboring lines are laterally offset
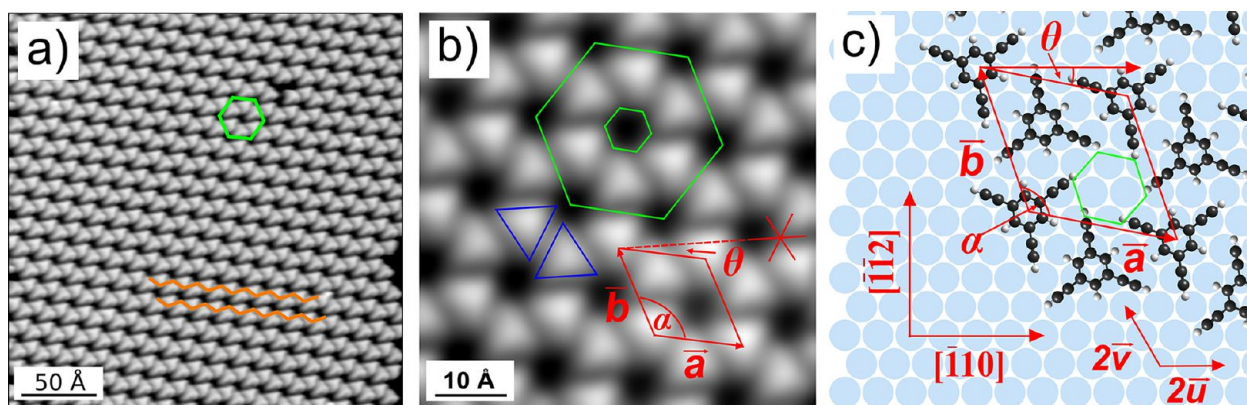
Figure 1. (a) STM topograph of TEB network ($U = -0.3$ V, $I = 0.1$ nA). (b) A zoomed image of the network with the corresponding elementary cell ($U = -0.1$ V, $I = 0.1$ nA). A small green hexagon represents a pore enclosed by hydrogen atoms of the respective molecules. (c) Model of the TEB network. The unit vectors $\vec{a}$ and $\vec{b}$ enclose the angle α. The angle θ is defined between the high-symmetry direction $[\bar{1}10]$ and $\vec{a}$. The primitive vectors of the Ag(111) surface are $\vec{u}$ and $\vec{v}$.

as indicated in Figure 1a. Three molecules from one zigzag line join three molecules from an adjacent line to construct a six-membered ring (green hexagon), which is enclosing a nanopore. From the uniform apparent height of the organic units and absence of a Moiré pattern, we conclude that the produced network is commensurate with the underlying atomic lattice. A zoomed image (Figure 1b) details that the building blocks can be identified as triangles (blue), each with one corner pointing oppositely with respect to the $[\bar{1}12]$ direction (defined in Figure 1c). Going along the direction from the center of the triangle to the center of the pore, every triangle is pointing left of the center of the pore, thus the superstructure exhibits organizational chirality.[47,48] Accordingly, the six-membered rings frame a chiral pore (small green hexagon in Figure 1b). Placing the corners of the pore at the tip terminations of the molecules, defined by an apparent height of 20% of the molecule's maximum apparent height, one can assign a maximal diameter $D_e = 5.8$ Å to the cavity. Domains with different principal directions and the opposite chirality as compared to those displayed in Figure 1 were also found on the substrate (Figure 2a,b).

The unit cell and its orientation with respect to the substrate (Figure 1b, red), as determined by atomically resolving the bare substrate, were obtained by averaging the values of four STM images (54×54 Å^2) recorded at the same area with different slow scanning directions to minimize the error caused by drift. The measured lengths of the vectors are $|\vec{a}| = |\vec{b}| = (13.1 \pm 0.3)$ Å and $\alpha = (119 \pm 1)°$. The angle θ between $\vec{a}$ and one of the $\langle \bar{1}10 \rangle$ high-symmetry directions (red star) is 11°.

Guided by the experimental values, we constructed the adsorption model depicted in Figure 1c with a ball-and-stick model of the molecules on the hexagonal Ag(111) lattice represented by blue circles. With the definition of the primitive vectors of the Ag(111) substrate given in Figure 1c, the elementary cell can be written in matrix representation as

$$\begin{pmatrix} \vec{a} \\ \vec{b} \end{pmatrix} = \begin{pmatrix} 4 & -1 \\ 1 & 5 \end{pmatrix} \begin{pmatrix} \vec{u} \\ \vec{v} \end{pmatrix}$$

With the nearest-neighbor distance of 2.89 Å, we obtain for the commensurate superstructure the values $|\vec{a}| = |\vec{b}| = 13.23$ Å, $\alpha = 120°$ and $\theta = 11°$, agreeing with the experimental findings within an error smaller than 1%. From the model it is obvious that the zigzag lines follow $\vec{a}$, while the offset between adjacent

lines is given by $\vec{b}$. The surface registry proposed by the model was not determined through experiments, because simultaneous molecular and atomic resolution was not achieved. Instead, we optimized the lateral displacement between the organic layer and the metal substrate to yield a highly symmetric arrangement. On the basis of this, we suggest that the centers of the phenyl moieties sit on hollow sites for which we can not distinguish between hexagonal close-packed (hcp) and face-centered cubic (fcc) ones, since we take into account the first substrate layer only.

An enlarged model (Figure 2c) highlights the enclosed pore and the supramolecular chiral organization. Placing the corners of the hexagon defining the cavity on top of the H atom centers, we find that the largest diameter of the hexagon amounts to $D_t = 5.78$ Å. Furthermore, the ethyne groups are not aligned with the bridge or top sites. By superposing a HYPERCHEM calculated model onto high-resolution STM data (see Supporting Information (SI), Figure S1), we found the best agreement for the molecular outlines assuming a rotation such that the terminal alkynes enclose an angle $\delta = (8 \pm 2)°$ with the $\langle \bar{1}12 \rangle$ directions and accordingly $(-8 \pm 2)°$ for the opposite chirality.

The rotation of the TEB molecule away from being oriented along the substrates high-symmetry directions is most likely originating from the intermolecular interaction of the terminal ethyne groups, but indirect substrate-mediated interaction could in principle also interfere. For a first, very simple analysis, we assume as the sole driving force an attraction between a terminal hydrogen atom and the center of the nearby ethyne group. We calculated the distance l between the two atom centers as a function of the angle δ. Interestingly, we found a parabola with a minimum at $\delta = 8°$ (Figure 2d), which nicely matches the STM data. Taking into account the oversimplifications of the assumed attraction, the quantitative agreement certainly cannot be regarded as conclusive. Nevertheless, this matching can be taken as a strong indication that the terminal ethyne groups are indeed the dominating driving force for the rotation of the molecules in the network.

In order to gain deeper understanding of the underlying interactions that drive the network formation, we carried out DFT calculations. In particular, we were interested in how the interplay between molecule−molecule and molecule-surface interactions affects the stability and the long-range order of the network. First, we studied the intermolecular interactions in gas
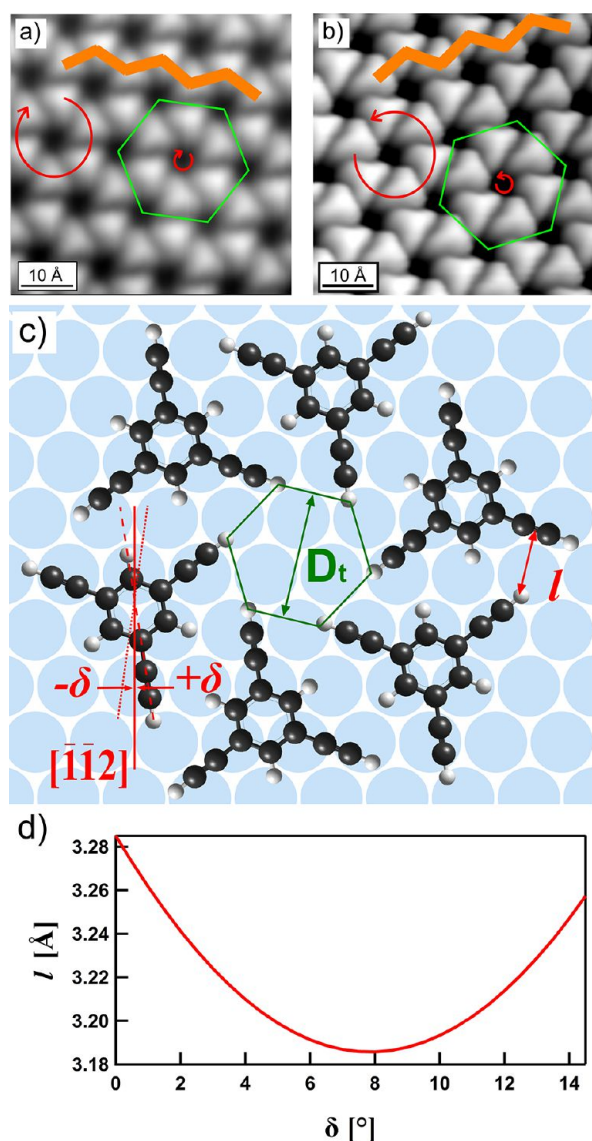
Figure 2. STM images of two different domains of ordered TEB networks showing (a) the left and (b) right enantiomorph. Brown zigzag lines show the two different principal directions that are correlated with the handedness. Green hexagons with corners at the center of the nanopores highlight the six-membered rings enclosing the chiral pores. The chiralities are denoted with red arrows. (c) Pore of a diameter D_t enclosed by terminal hydrogen atoms (green), distance from a terminal hydrogen atom to the center of ethyne group on the nearest-neighbor molecule l, and the angle δ describing the rotation away from the $[1\bar{1}2]$ direction (red). (d) Ethyne bonding distance l as a function of the angle δ.

phase calculations of a TEB dimer (Figure 3a) and the periodic TEB network (Figure 3b). For the TEB network, both the internal structure and the length of the unit cell vectors were optimized while $\alpha = 120°$ was kept constant. To compare the bonding strength between dimer and network, we define the binding energy of a molecule per molecule–molecule interaction for the dimer as

$$E_{\text{bind,dim}} = -(E_{\text{dim}} - 2E_{\text{mol}})$$
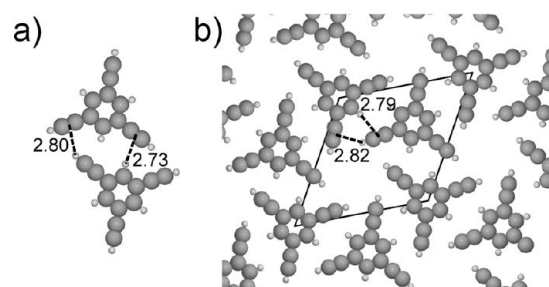
and for the network as

Figure 3. (a) Gas phase dimer. (b) Network made of TEB molecules with the corresponding distances in angstroms.

$$E_{\text{bind,net}} = -\frac{E_{\text{net}} - 2E_{\text{mol}}}{3}$$

where E_{mol}, E_{dim}, and E_{net} are the total energies per unit cell of the TEB molecule, the TEB dimer, and the TEB network, respectively, on the surface. The denominator 3 is due to the fact that in the network each molecule is interacting with three surrounding ones, whereas the factor 2 describes two molecules per elementary cell. In our theoretical framework, a more negative energy of a single parameter (E_{mol}, E_{dim}, or E_{net}) means a more stable situation, while a positive binding energy (E_{bind}) is associated with stabilization due to the interaction of the isolated parts. $E_{\text{bind,dim}}$ and $E_{\text{bind,net}}$ amount to 0.20 and 0.22 eV, respectively, hence the strengths per molecule–molecule interaction are comparable and the long-range order of the network has no recognizable cooperative effect on the individual interactions. The energy gained per molecule by formation of the periodic 2D sheet is

$$E_{\text{form}} = -\frac{E_{\text{net}} - 2E_{\text{mol}}}{2} = 0.33 \text{ eV}$$

For the isolated molecular sheet, the optimized length of the two unit cell vectors is 12.77 Å, hence theory predicts an optimal lattice constant of almost 0.5 Å shorter than the one experimentally observed. We attribute the difference to the molecule–surface interaction, which obviously has a great influence on the self-assembly of TEB on Ag(111). Thus, in the next step of our DFT analysis, we explicitly take into account the substrate. For the adsorption of a single TEB molecule on Ag(111) four high-symmetric adsorption geometries were found as local minima (see SI, Figure S2). Notably, the adsorption energy gain, E_{ad}, varies significantly between the different cases and ranges from 1.40 to 1.19 eV from the most to the least stable configuration, respectively. This difference is of the same order of magnitude as E_{form}. Thus the surface is expected to pin the molecules to positions of well-defined registry in agreement with the experimental finding of the formation of a commensurable, long-range ordered network.

In Figure 4a,b the two most stable adsorption configurations of TEB on Ag(111) are depicted. In both cases, the phenyl ring is centered above a hollow site, while the ethyne triple bonds are aligned with bridge and on top positions as depicted in Figures 4a and b, respectively. Note that FCC and HCP hollow sites were indistinguishable, with energy differences smaller than 5 meV. Figure 4c illustrates the most stable geometry for the TEB network on the Ag(111) surface determined under the constraint of the model unit cell. Other configurations of networks representing local energy minima are given in the SI, Figure S3. The superstructure can be understood as consisting of entities alternatively adopting the two most stable geometries
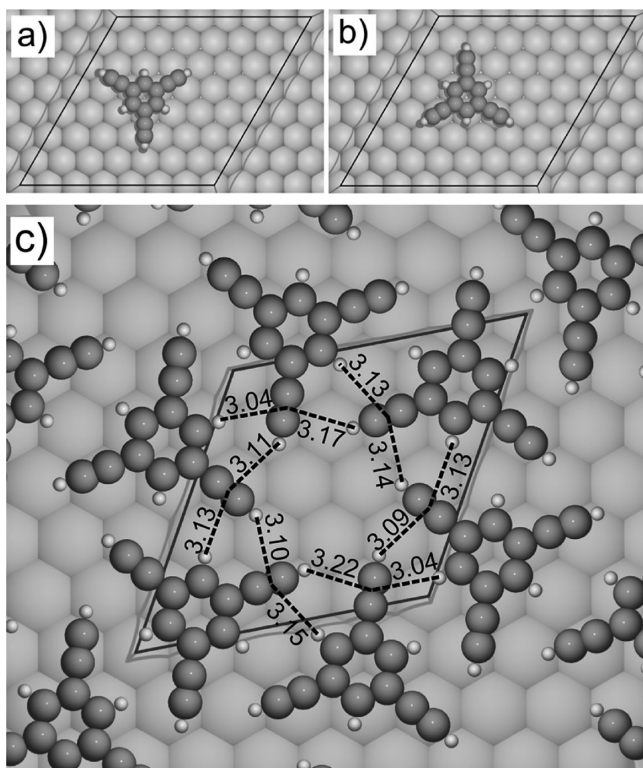
3990

dx.doi.org/10.1021/jp310606r | *J. Phys. Chem. C* 2013, 117, 3987−3995

Figure 4. DFT optimized adsorption geometries of isolated molecules and the periodic network. Black lines indicate the surface unit cell used in the calculations. (a,b) Isolated TEB units adsorb on Ag(111) in a highly symmetric manner. (a) In the second most stable situation (E_{ad} = 1.26 eV) the phenyl moiety is centered over fcc hollow site and terminal alkynes are over bridge positions. (b) Most stable registry (E_{ad} = 1.40 eV) with the phenyl center over hcp hollow site and alkynes over on top positions. (c) The geometry of the entire network is characterized by molecules being centered over hollow sites with terminal alkynes rotated away from the original bridge and on top alignment. Note that the enantiomorph opposite to the one of the experimental model (Figure 1c) is depicted.

for the single molecules. However, all molecules are rotated imprinting chirality to the nanoporous phase, whereby the rotation angle $\alpha = 8°$ is in excellent agreement with the experiments. From the comparison of the adsorption configurations of the single organic units and the periodic assembly, it is obvious that the rotation results from the intermolecular attraction focused on the terminal alkynes generating a torque around the phenyl ring centers, which are pinned at hollow sites of the substrate. In Figure 4c the distances between the centers of ethyne triple bonds and nearby hydrogen atoms are also indicated. Compared to the isolated organic sheet (Figure 3b), the intermolecular bonding distances are substantially larger under on-surface conditions, due to the commensurability with the Ag(111) surface putting a constraint on the intermolecular distances. We calculated the energy gained per molecule by formation of the network on the surface by

$$E_{form,sub} = -\frac{E_{net,sub} - 2E_{mol} - E_{sub}}{2} - E_{ad}$$

where $E_{net,sub}$ and E_{sub} are the total energies per unit cell for the network on the surface and the clean surface, respectively. We found a stabilization by 0.11 eV/molecule with respect to the single molecules on the substrate, while for the isolated organic

sheet E_{form} is 0.33 eV/molecule. The smaller energy gain on the surface has two origins. First, due to the commensurability of the network with the surface, discussed above, the intermolecular distances are restricted to a regime in which $E_{bind,net}$ has not yet reached its maximum. Second, the adsorption configuration of each molecule in the superstructure is disrupted from the corresponding most favorable geometry reducing E_{ad}. The rotation-induced lowering of E_{ad} is reflected in the fact that the average adsorption heights for an isolated molecule and a molecule integrated in the network are 2.93 Å and 3.15 Å, respectively. In other words, there is a very delicate balance of energy gain due to intermolecular interactions and loss by disrupting molecule−surface interactions that control the on-surface network formation.

A delicate aspect of the adsorption of conjugated organic molecules on metal surfaces is the correct description of the surface bonding energy. Recent work on this topic[49−51] demonstrates that this is still a challenging task and requires the most advanced DFT+vdW approaches to even get near to a quantitative depiction of the real physics. Therefore it is necessary to analyze the role of the vdW interactions in the TEB network formation and to understand how good our theory performs in describing it. We use the experimental desorption temperature as a measure of performance. As detailed later in the text we found that TEB desorbs around 280−300 K. For an estimation of the desorption activation energy, E_{des}, following from this temperature we assume that an average desorption rate, ν_{des}, of approximately 0.001 s^{-1} is sufficient to desorb TEB during annealing to T_{des} = 300 K. Relating the two quantities via the Arrhenius expression

$$\nu_{des} = A_0 \cdot \exp\left(\frac{-E_{des}}{k_B T}\right)$$

where k_B is the Boltzmann constant, and assuming a prefactor $A_0 = 10^{13}$ s^{-1} we obtain

$$E_{des} = \ln\left(\frac{A_0}{\nu_{des}}\right) k_B T_{des} = 0.95 \text{ eV}$$

which value needs to be reconciled with theory.

Our results were obtained using the fully nonlocal van der Waals density functional combined with the optimized form of Becke 86 exchange (vdWDF/optB86b).[46] For comparison, we also performed calculations without vdW interactions using the semilocal Perdew−Burke−Ernzerhof (PBE) functional[52] and with the most common vdW correction proposed by Grimme in 2006.[53] For the isolated TEB on Ag(111), using the adsorption configuration depicted in Figure 4b, the PBE functional gives a binding energy of only 0.11 eV, while the Grimme and our approach give 1.66 and 1.40 eV, respectively. Thus, the binding to the surface is primarily established by vdW interactions, and, even though overestimating the bonding strength, our method provides a more accurate binding energy than the Grimme alternative.

Next we analyze the influence of the vdW forces on the intermolecular interactions leading to the self-assembly. For the freestanding TEB network (without surface), PBE gives a network formation gain of 0.13 eV per molecule. This should be compared to 0.33 eV for vdWDF/optB86b, showing that the vdW interactions are important also for stabilizing the network. Now, considering the TEB network on Ag(111), PBE gives a lateral stabilization energy of 0.07 eV per molecule with respect to

to the isolated species on the surface, while the corresponding value for vdWDF/optB86b is 0.11 eV. Thus, on the surface, the calculations with and without vdW interactions give very similar formation energies, and this has two origins. As mentioned above, the network formation energy includes both the energy gain from intermolecular interaction, as well as the energy cost for disrupting the optimal molecule−surface interaction. The similar formation energies given by vdWDF/optB86b and PBE are solely due to cancelation between these two effects.

In conclusion, vdW interactions are important both for the molecule−surface and molecule−molecule interactions guiding the self-assembly of TEB on the Ag(111) surface. Our results show that by using vdWDF/optB86b, a good qualitative description of the hierarchy between molecule−molecule and molecule−surface interactions can be obtained and that the rotation of the molecules as well as the network formation itself are correctly predicted. Thus, even though overestimating the surface bonding energy, we suggest that this methodology is helpful for the analysis of similar types of systems.

Next we analyze the stabilization of the superstructure in terms of distinct bonds. Figure 5 shows a charge difference plot
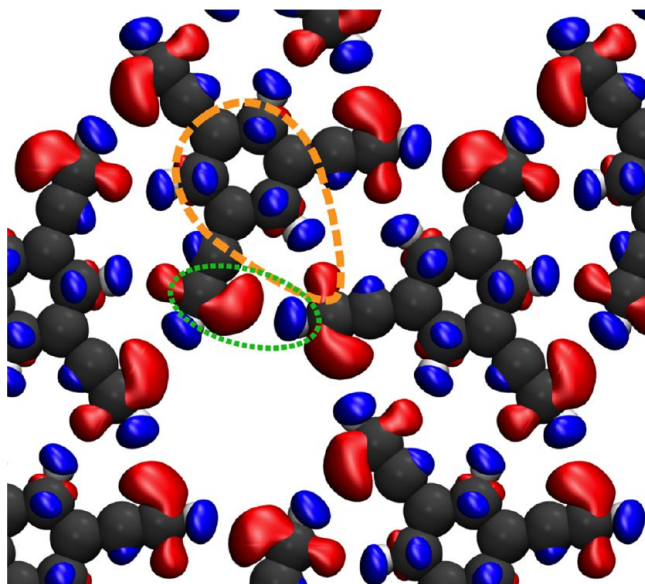

Figure 5. Electron charge difference plot of the TEB network in gas phase illustrating the redistribution of the electronic density induced by the network formation. The absolute value of the contours is 0.001e, where red is electron accumulation and blue is electron depletion.

of an isolated TEB sheet, illustrating the electron accumulation (red) and depletion (blue) induced by the formation of the network as compared to noninteracting gas phase molecules. The intermolecular bonding in the TEB network is mainly characterized by two types of noncovalent bonding motifs. One is a weak H-bond between ethyne groups (green dotted ellipse) indicated by accumulation of electron charge around the ethyne group donating its π-system to the hydrogen bridge and depletion of electrons around the H atom donated by the other ethyne group. For the second intermolecular contact, namely, again between an ethyne π-system and the nearby methine unit of the neighboring phenyl moiety, we suggest the proton acceptor ring interaction (PARI)[54] as the driving force. As demonstrated very recently,[54] the in-plane interaction between a functional group bearing the potential to act as a proton

acceptor in a H bridge and a benzene ring presents a special case of hydrogen bonding.[55] This is because the major part of the complexation energy gain is not originating from the methine unit near to the proton acceptor, but from the more remote half of the benzene ring. In the PARI situation, the proton acceptor is pointing with its electron lone pair toward the benzene ring. Considering the geometry of the ethyne π-system in the case discussed here, the charge difference plot reveals a great similarity, and, accordingly, we attribute the second contact to a PARI. The interpretation that mainly the in-plane π-orbitals contribute to the bonding mechanism is further corroborated by the projected density of states (PDOS) displayed in Figure S4. For the TEB network on the surface, very similar charge difference behavior was found (Figure S5a), indicating that the bonding mechanism preserves its character with the presence of the noble metal substrate.

In order to estimate how much each of the two bonding motifs contribute to the overall binding, we constructed an alternative dimer featuring only the PARI (Figure S5b) and compared it to a normal dimer with ethyne−ethyne H bridge and PARI (Figure S5c). The binding energy of the modified dimer is 0.10 eV, hence half the binding energy of a normal TEB dimer. In other words, in the dimer, the PARI contributes significantly to the stabilization. The PARI-related binding energy agrees well with what is expected for a PARI originating from benzene.[54] Even though the PARI contribution is significant, the ethyne−ethyne interaction is expected to have a major influence on the overall network stabilization. This can be explained by different distances between the ethyne group and the benzene H-atom. Namely, in the TEB network, this distance is larger than in the alternative dimer with only PARIs. Hence, we conclude that the PARI contribution is somewhat weakened by introducing the ethyne−ethyne interactions.

In the following, we compare with ethyne-related ordering in a 3D environment. It is noteworthy that in the case of bulk material, the ordering of the molecules featuring terminal alkynes often exhibits folded layer structure.[10,12−15,17,18,20] A six-membered cyclic binding motif was reported before,[17] but the alkynes are not laying in the same plane and are rather pointing in the opposite directions orthogonal to the plane that contains the binding motif. To the best of our knowledge, no indication for appreciable in-plane interactions between ethyne and phenyl moieties have been reported so far. Note that in-plane geometry is a completely different case than the well-established hydrogen bridge between a proton-donating ethyne group and the π-system of a benzene ring.[12,20] Thus the planarity and the PARI contribution to the stabilization qualify our binding six-membered cyclic binding motif as a novel synthon.

As a generalization step in our study of terminal alkyne-related self-assembly, we synthesized Ext-TEB (Scheme 1). This molecule also exhibits 3-fold symmetry, but features additional benzene rings between the central one and the terminal ethyne groups. The H−H distance of the terminal groups is 16.27 Å. After Ext-TEB was deposited onto the Ag(111) surface (T_{sample} = 156 K), two different supramolecular arrangements coexist, namely, a compact (CP, Figure 6a) and an open-porous (OP, Figure 7a) phase. Both phases form large domains of high-quality. The CP is very similar to the network made by TEB-molecules, again with a principal direction highlighted by zigzag chains (orange) in Figure 6a. Also, six-membered rings (green) enclose a nanopore. A close inspection of a zoomed-in image (Figure 6b) reveals in close analogy to
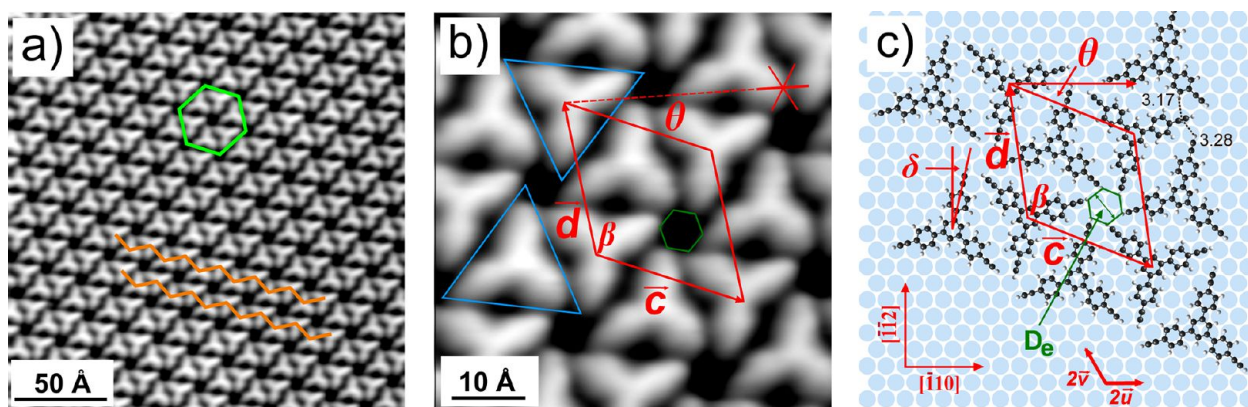
Figure 6. CP phase of the Ext-TEB network. (a) Large-scale STM topograph showing a long-range ordering of the supramolecular network ($U = -0.09$ V, $I = 0.05$ nA). (b) A zoomed image of the network with the corresponding elementary cell ($U = -0.09$ V, $I = 0.05$ nA). (c) Model of the CP phase.
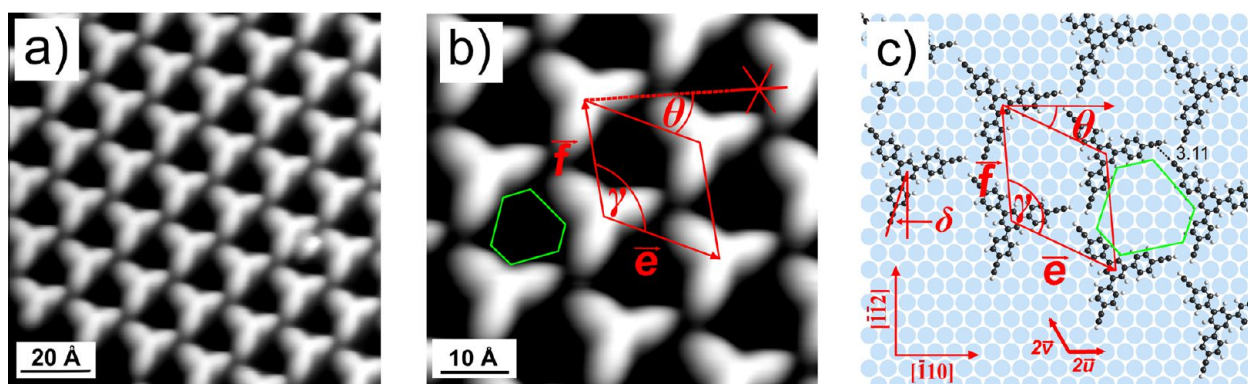

Figure 7. OP phase of the Ext-TEB network. (a) Large-scale STM topograph showing a long-range ordering of the supramolecular network ($U = -0.09$ V, $I = 0.05$ nA). (b) A zoomed image of the network with the corresponding elementary cell ($U = -0.09$ V, $I = 0.05$ nA). (c) Ball-and-stick network model.

the case of TEB that two types of molecules (blue triangles pointing in different $\langle \bar{1}10 \rangle$ directions) are present in the superstructure, and that the terminal groups are pointing left of the pore center, thus the pores are chiral. The rotation angle is $\delta = (13 \pm 1)°$. The diameter of a pore amounts to $D_e = 4.8$ Å, i.e., slightly reduced compared to the smaller tecton. Ext-TEB builds up a periodic layer with a rhombic elementary cell. The experimentally determined values for the unit cell are $|\vec{c}| = |\vec{d}| = (20.0 \pm 0.4)$ Å, angle $\beta = (119.1 \pm 0.4)°$, $\theta = 22°$ (Figure 6b). Within an error of approximately 1%, we propose a commensurate one defined by $|\vec{c}| = |\vec{d}| = 20.22$ Å, $\beta = 120°$, $\theta = 21.79°$, which is given in matrix representation as

$$\begin{pmatrix} \vec{c} \\ \vec{d} \end{pmatrix} = \begin{pmatrix} 5 & -3 \\ 3 & 8 \end{pmatrix} \begin{pmatrix} \vec{u} \\ \vec{v} \end{pmatrix}$$

with reference to the silver surface basis vectors $\vec{u}$ and $\vec{v}$. With the same definition as in the TEB assembly, the maximal pore hexagon diameter amounts to $D_e = 4.76$ Å. Again, the surface registry was unknown, but through symmetry optimizing, we were able to construct a commensurate supramolecular model (Figure 6c), which fits well to the measured data and where the constituents have a well-defined registry with the substrate. We propose that for one molecule type, the central aromatic ring is placed on top while the outer rings adopt hollow site, whereas for the other type the registry is inverted. Without further arguments from DFT calculations, we conclude from the

pronounced similarity of the circular binding motifs around the pores (cf. Figure 1c and Figure 6c) that also the interactions contributing to the network stabilization carry similar properties. The hydrogen bonds established by the ethyne groups have an average length of 3 Å, and the PARI-type bonds manifest with a binding length of 3.17 Å.

Contrary to the two previous arrangements, in the OP, all molecules have the same orientation (Figure 7a). Only three ethyne groups (Figure 7b,c) are contributing to the nodal connections between organic units, and no pore is enclosed by them. Instead, a larger pore (green) is present in between the molecules. Due to the chirality of the nodal motif, the pores can be understood as 3-fold symmetric hexagons featuring three long and three short sides (as depicted in Figure 7b,c). Similarly to the previous structures, the complete network can be constructed by successive translations of the rhombic unit cell ($|\vec{e}| = |\vec{f}| = (17.3 \pm 0.4)$ Å, $\gamma = (119 \pm 1)°$ $\theta = (26 \pm 1)°$) defined in Figure 7b. The rotation angle δ for this structure amounts to $(18 \pm 2)°$. Within an error of 1.3%, we translate the experimental values into a commensurate model superstructure ($|\vec{e}| = |\vec{f}| = 17.57$ Å, $\gamma = 120°$, $\theta = 25.29°$), which has the matrix notation

$$\begin{pmatrix} \vec{e} \\ \vec{f} \end{pmatrix} = \begin{pmatrix} 4 & -3 \\ 3 & 7 \end{pmatrix} \begin{pmatrix} \vec{u} \\ \vec{v} \end{pmatrix}$$

Again, for symmetry reasons, we propose that the central benzene ring is centered above an on top site, while the centers of the three outer phenyl units are positioned over hollow sites (Figure 7c). The OP is also different than the two others with respect to the interactions present. Here each terminal alkyne contributes in two ethyne–ethyne bonds only, but does not connect to a benzene ring. Since the hydrogen bridge lengths (3.14 Å) are approximately the same as that for the other networks on the surface, we believe that the binding energies related to it are also similar. Accordingly, we suggest that the OP is energetically less favorable than the CP due to the missing PARI.

Furthermore, it is interesting to explore the high temperature behavior of the molecules. Upon annealing to higher temperatures we found the desorption of TEB to take place in the temperature range 270–300 K. On the contrary, after the annealing of samples with a submonolayer coverage of Ext-TEB to 300 K, novel molecular units, i.e., dimers, are present. Further annealing to 400 K results in irregular networks. From the room temperature stability of these structures, we conclude that covalent bonding is the predominant mechanism responsible for their formation, and we attribute these effects to the interplay of the reactive terminal alkynes with the catalytic metal substrate.[41]

CONCLUSION

In conclusion, we studied the self-assembly capabilities of two 3-fold symmetric organic species with aromatic backbones and terminal alkyne groups on Ag(111). We found long-range ordered commensurate networks and were able to understand the underlying balance between the intermolecular forces and the molecule–substrate interaction in great detail. The superstructures exhibit organizational chirality and are stabilized by a novel, six-membered cyclic synthon, where the ethyne–ethyne interaction is dominant and which is a planarized variant of ethyne-related binding motifs appearing in 3D environments. However, under on-surface conditions, a substantial part of the stabilization is provided by the interaction between terminal alkyne groups and the phenyl units of neighboring molecules, a characteristic that is absent without substrate. No appreciable cooperative effects were found in the periodic organic sheets. In addition, for the larger species a loosely packed phase was found with a 3-fold binding motif being more similar to the known 3D synthons. Our work demonstrates that terminal alkyne groups can be used for the rational bottom-up construction of on-surface hydrocarbon networks and related nanoarchitectures.

ASSOCIATED CONTENT

Ⓢ Supporting Information

A picture of the TEB network model superimposed on the STM topograph is given as well as the four energetically most favorable adsorption configurations of the isolated TEB molecule. Furthermore, a comparison of six different network geometries is presented. We also provide information on the dimer bonding and the network on the surface by showing PDOS and electron charge differences. This material is available free of charge via the Internet at http://pubs.acs.org.

AUTHOR INFORMATION

Corresponding Author

*E-mail: florian.klappenberger@tum.de.

Notes

The authors declare no competing financial interest.

REFERENCES

(1) Prins, L. J.; Reinhoudt, D. N.; Timmerman, P. *Angew. Chem., Int. Ed.* **2001**, *40*, 2383–2426.
(2) Lehn, J. M. *Proc. Natl. Acad. Sci. U.S.A.* **2002**, *99*, 4763–4768.
(3) Ariga, K.; Lee, M. V.; Mori, T.; Yu, X. Y.; Hill, J. P. *Adv. Colloid Interface Sci.* **2010**, *154*, 20–29.
(4) Desiraju, G. R. *Acc. Chem. Res.* **2002**, *35*, 565–573.
(5) Steiner, T. *Angew. Chem., Int. Ed.* **2002**, *41*, 48–76.
(6) Desiraju, G. R. *Angew. Chem., Int. Ed. Engl.* **1995**, *34*, 2311–2327.
(7) Desiraju, G. R. *Chem. Commun.* **1997**, 1475–1482.
(8) Nishio, M. *CrystEngComm* **2004**, *6*, 130–158.
(9) Nishio, M. *Phys. Chem. Chem. Phys.* **2011**, *13*, 13873–13900.
(10) Steiner, T. *J. Chem. Soc., Chem. Commun.* **1995**, 95–96.
(11) Benghiat, V.; Leiserowitz, L. *J. Chem. Soc., Perkin Trans. 2* **1972**, 1772–1778.
(12) Steiner, T.; Starikov, E. B.; Amado, A. M.; Teixeiradias, J. J. C. *J. Chem. Soc., Perkin Trans. 2* **1995**, 1321–1326.
(13) Steiner, T.; Starikov, E. B.; Tamm, M. *J. Chem. Soc., Perkin Trans. 2* **1996**, 67–71.
(14) Weiss, H. C.; Bläser, D.; Boese, R.; Doughan, B. M.; Haley, M. M. *Chem. Commun.* **1997**, 1703.
(15) Robinson, J. M. A.; Kariuki, B. M.; Gough, R. J.; Harris, K. D. M.; Philp, D. *J. Solid State Chem.* **1997**, *134*, 203–206.
(16) Kumar, S.; Subramanian, K.; Srinivasan, R.; Rajagopalan, K.; Steiner, T. *J. Mol. Struct.* **1998**, *471*, 251–255.
(17) Steiner, T.; Tamm, M.; Grzegorzewski, A.; Schulte, N.; Veldman, N.; Schreurs, A. M. M.; Kanters, J. A.; Kroon, J.; van der Maas, J.; Lutz, B. *J. Chem. Soc., Perkin Trans. 2* **1996**, 2441–2446.
(18) Saha, B. K.; Nangia, A. *Cryst. Growth Des.* **2007**, *7*, 393–401.
(19) Jeffrey, G. A.; Saenger, W. *Hydrogen Bonding in Biological Structures*; Springer: Berlin, 1991.
(20) Steiner, T.; Tamm, M.; Lutz, B.; van der Maas, J. *Chem. Commun.* **1996**, 1127–1128.
(21) Kumar, S.; Subramanian, K.; Srinivasan, R.; Rajagopalan, K.; Schreurs, A. M. M.; Kroon, J.; Koellner, G.; Steiner, T. *J. Mol. Struct.* **1998**, *448*, 51–55.
(22) Philp, D.; Robinson, J. M. A. *J. Chem. Soc., Perkin Trans. 2* **1998**, 1643–1650.
(23) Barth, J. V. *Annu. Rev. Phys. Chem.* **2007**, *58*, 375–407.
(24) Elemans, J. A. A. W.; Lei, S. B.; De Feyter, S. *Angew. Chem., Int. Ed.* **2009**, *48*, 7298–7332.
(25) Kudernac, T.; Lei, S. B.; Elemans, J. A. A. W.; De Feyter, S. *Chem. Soc. Rev.* **2009**, *38*, 402–421.
(26) Barth, J. V.; Weckesser, J.; Cai, C. Z.; Günter, P.; Bürgi, L.; Jeandupeux, O.; Kern, K. *Ang. Chem., Int. Ed.* **2000**, *39*, 1230–1234.
(27) Furukawa, M.; Tanaka, H.; Kawai, T. *Surf. Sci.* **2000**, *445*, 1–10.
(28) Otero, R.; Schock, M.; Molina, L. M.; Laegsgaard, E.; Stensgaard, I.; Hammer, B.; Besenbacher, F. *Angew. Chem., Int. Ed.* **2005**, *44*, 2270–2275.
(29) Dmitriev, A.; Lin, N.; Weckesser, J.; Barth, J.; Kern, K. *J. Phys. Chem. B* **2002**, *106*, 6907–6912.
(30) Griessl, S.; Lackinger, M.; Edelwirth, M.; Hietschold, M.; Heckl, W. M. *Single Mol.* **2002**, *3*, 25–31.

(31) Theobald, J. A.; Oxtoby, N. S.; Phillips, M. A.; Champness, N. R.; Beton, P. H. *Nature* **2003**, *424*, 1029−1031.

(32) Cañas-Ventura, M. E.; Xiao, W.; Wasserfallen, D.; Müllen, K.; Brune, H.; Barth, J. V.; Fasel, R. *Angew. Chem., Int. Ed.* **2007**, *46*, 1814−1818.

(33) Yokoyama, T.; Kamikado, T.; Yokoyama, S.; Mashiko, S. *J. Chem. Phys.* **2004**, *121*, 11993−11997.

(34) Yokoyama, T.; Yokoyama, S.; Kamikado, T.; Okuno, Y.; Mashiko, S. *Nature* **2001**, *413*, 619−621.

(35) Schlickum, U.; Decker, R.; Klappenberger, F.; Zoppellaro, G.; Klyatskaya, S.; Auwärter, W.; Neppl, S.; Kern, K.; Brune, H.; Ruben, M.; et al. *J. Am. Chem. Soc.* **2008**, *130*, 11776−11782.

(36) Kühne, D.; Klappenberger, F.; Decker, R.; Schlickum, U.; Brune, H.; Klyatskaya, S.; Ruben, M.; Barth, J. V. *J. Phys. Chem. C* **2009**, *113*, 17851−17859.

(37) Li, Q.; Han, C. B.; Horton, S. R.; Fuentes-Cabrera, M.; Sumpter, B. G.; Lu, W. C.; Bernholc, J.; Maksymovych, P.; Pan, M. H. *ACS Nano* **2012**, *6*, 566−572.

(38) Polzonetti, G.; Carravetta, V.; Russo, M. V.; Contini, G.; Parent, P.; Laffon, C. *J. Electron Spectrosc. Relat. Phenom.* **1999**, *99*, 175−187.

(39) Iucci, G.; Carravetta, V.; Altamura, P.; Russo, M. V.; Paolucci, G.; Goldoni, A.; Polzonetti, G. *Chem. Phys.* **2004**, *302*, 43−52.

(40) Sohn, Y.; Wei, W.; White, J. M. *J. Phys. Chem. C* **2007**, *111*, 5101−5110.

(41) Zhang, Y.-Q.; Kepčija, N.; Kleinschrodt, M.; Diller, K.; Fischer, S.; Papageorgiou, A. C.; Allegretti, F.; Björk, J.; Klyatskaya, S.; Klappenberger, F.; et al. *Nat. Commun.* **2012**, *3*, 1286.

(42) Kresse, G.; Furthmuller, J. *Phys. Rev. B* **1996**, *54*, 11169−11186.

(43) Blöchl, P. E. *Phys. Rev. B* **1994**, *50*, 17953−17979.

(44) Kresse, G.; Joubert, D. *Phys. Rev. B* **1999**, *59*, 1758−1775.

(45) Dion, M.; Rydberg, H.; Schroder, E.; Langreth, D.; Lundqvist, B. *Phys. Rev. Lett.* **2004**, *92*, 246401−246404.

(46) Klimeš, J.; Bowler, D. R.; Michaelides, A. *Phys. Rev. B* **2011**, *83*, 195131.

(47) Ecija, D.; Trelka, M.; Urban, C.; de Mendoza, P.; Mateo-Marti, E.; Rogero, C.; Martin-Gago, J. A.; Echavarren, A. M.; Otero, R.; Gallego, J. M.; et al. *J. Phys. Chem. C* **2008**, *112*, 8988−8994.

(48) Bombis, C.; Weigelt, S.; Knudsen, M. M.; Norgaard, M.; Busse, C.; Laegsgaard, E.; Besenbacher, F.; Gothelf, K. V.; Linderoth, T. R. *ACS Nano* **2010**, *4*, 297−311.

(49) Björk, J.; Hanke, F.; Palma, C. A.; Samori, P.; Cecchini, M.; Persson, M. *J. Phys. Chem. Lett.* **2010**, *1*, 3407−3412.

(50) Ruiz, V. G.; Liu, W.; Zojer, E.; Scheffler, M.; Tkatchenko, A. *Phys. Rev. Lett.* **2012**, *108*, 146103.

(51) Simpson, S.; Zurek, E. *J. Phys. Chem. C* **2012**, *116*, 12636−12643.

(52) Perdew, J. P.; Burke, K.; Ernzerhof, M. *Phys. Rev. Lett.* **1996**, *77*, 3865−3868.

(53) Grimme, S. *J. Comput. Chem.* **2006**, *27*, 1787−1799.

(54) Arras, E.; Seitsonen, A. P.; Klappenberger, F.; Barth, J. V. *Phys. Chem. Chem. Phys.* **2012**, *14*, 15995−16001.

(55) Arunan, E.; Desiraju, G. R.; Klein, A. R.; Sadlej, J.; Scheiner, S.; Alkorta, I.; Clary, D. C.; Crabtree, R. H.; Dannenberg, J. J.; Hobza, P.; et al. *Pure Appl. Chem.* **2011**, *83*, 1637−1641.